EJN European Journal of Neuroscience

FENS Federation of European Neuroscience Societies

European Journal of Neuroscience, Vol. 42, pp. 3066–3080, 2015 doi:10.1111/ejn.13104

MOLECULAR AND SYNAPTIC MECHANISMS

Copper enhances cellular and network excitabilities, and improves temporal processing in the rat hippocampus

Carlos Maureira, Juan Carlos Letelier, Osvaldo Alvarez, Ricardo Delgado and Cecilia Vergara
Departamento de Biología, Facultad de Ciencias, Universidad de Chile, Casilla 653, Santiago 7800003, Chile

Keywords: copper, correlation, hippocampus, inhibition, neuronal excitability, reliability

Edited by Paul Bolam
Received 4 September 2015, accepted 3 October 2015

Abstract

Copper, an ion with many important metabolic functions, has also been proposed to have a role as modulator on neuronal function, mostly based on its effects on voltage- and neurotransmitter-gated conductance as well as on neurological symptoms of patients with altered copper homeostasis. Nevertheless, the mechanisms by which copper exerts its neuromodulatory effects have not been clearly established in a functional neuronal network. Using rat hippocampus slices as a neuronal network model, the effects of copper in the range of 10–100 nM were tested on the intrinsic, synaptic and network properties of the CA1 region. Most of the previously described effects of this cation were in the micromolar range of copper concentrations. The current results indicate that copper is a multifaceted neuromodulator, having effects that may be grouped into two categories: (i) activity enhancement, by modulating synaptic communication and action potential (AP) conductances; and (ii) temporal processing and correlation extraction, by improving reliability and depressing inhibition. Specifically it was found that copper hyperpolarizes AP firing threshold, enhances neuronal and network excitability, modifies CA3–CA1 pathway gain, enhances the frequency of spontaneous synaptic events, decreases inhibitory network activity, and improves AP timing reliability. Moreover, copper chelation by bathocuproine decreases spontaneous network spiking activity. These results allow the proposal that copper affects the network activity from cellular to circuit levels on a moment-by-moment basis, and should be considered a crucial functional component of hippocampal neuronal circuitry.

Introduction

Copper has many metabolic functions in aerobic cells, and it has been proposed to have a role as neuromodulator (Prohaska, 1987; Lalioti *et al.*, 2009; Banci *et al.*, 2010; Lutsenko, 2010). Brain copper concentration is highly controlled (Lutsenko, 2010; Lutsenko *et al.*, 2010), and divided into a tightly bound pool and rapidly recycling or labile pool (Pase *et al.*, 2004; Schlief *et al.*, 2005). Copper is found in synaptic and somatic vesicles, and is released by synaptic and extra-synaptic mechanisms (Kozma *et al.*, 1981; Hartter & Barnea, 1988; Hopt *et al.*, 2003; Schlief & Gitlin, 2006; Gaier *et al.*, 2013). In addition, it is unevenly distributed in the adult CNS (Lalioti *et al.*, 2009; Davies *et al.*, 2013) and differentially regulated during development (Saito *et al.*, 1995; Tarohda *et al.*, 2004; Niciu *et al.*, 2006).

Abnormal CNS copper levels are associated with Menkes and Wilson's diseases, characterized by severe neurological alterations (de Bie *et al.*, 2007; Zatta & Frank, 2007; Vogt & Ralle, 2013). Chelation therapy can either alleviate or exacerbate neuropsychiatric aspects of Wilson's disease, supporting the idea that the rapidly recycling copper pool regulates neural activity (Pase *et al.*, 2004; Gaier *et al.*, 2013). Nevertheless, how copper interacts with specific nuclei within the CNS is not well understood (Que *et al.*, 2008; Lutsenko, 2010; Lutsenko *et al.*, 2010; Gaier *et al.*, 2013). Copper concentrations in cerebrospinal fluid (CSF) have been reported to be between 130 and 600 nM (Gaier *et al.*, 2013), while estimations of copper concentration in the synaptic space range from 15 to 250 μM (Hartter & Barnea, 1988; Kardos *et al.*, 1989; Herms *et al.*, 1999). At high-micromolar ranges (~ 100 μM), copper blocks sodium, calcium, potassium channels, γ-aminobutyric acid $(GABA)_A$ receptors, AMPA receptors, *N*-methyl-D-aspartate receptors and purinergic receptors (Gruss *et al.*, 2004; Huidobro-Toro *et al.*, 2008). However, at lower concentrations (0.1–3 μM), copper activates TREK-1 background K^+ channel, P2X2 purinergic receptor and sodium channels from toad olfactory neurons (Gruss *et al.*, 2004; Lorca *et al.*, 2005; Delgado *et al.*, 2006). Nanomolar copper concentrations block $GABA_A$ currents in dissociated Purkinje neurons (IC_{50} 35 nM; Sharonova *et al.*, 1998, 2000). In toad olfactory epithelia dissociated cells, 100 nM copper triggered an acceleration of the activation and inactivation rates of the sodium currents and increased intrinsic neuronal excitability, but at 1 μM inhibition of action potential (AP) firing is observed (Aedo *et al.*, 2007). In addition, copper functional roles include resetting of circadian clock phase (Yamada & Prosser, 2014) and fear-related behaviours involving the amygdala (Gaier

Correspondence: Dr Carlos Maureira and Dr Cecilia Vergara, as above.
E-mails: carlos.maureira@uchile.cl and cvergara@uchile.cl

et al., 2014a,b). Considering that membrane receptors and ion channels are affected by copper, it was hypothesized that copper could modulate CNS excitability targeting the initiation and propagation of APs as well as synaptic transmission. By affecting these parameters, copper could modulate the activity of the neural network. To explore this hypothesis, the effects of nanomolar copper in hippocampal slices were characterized, a system that preserves its synaptic connectivity and whose properties are well known. It was found that nanomolar copper concentrations can fine-tune hippocampal microcircuits by regulating intrinsic cell excitability, synaptic and network mechanisms, and therefore could have a wide impact on neural functions. Thus, it was proposed that copper acts as a multifaceted neuromodulator, a role that could also shed light on the mechanisms underlying copper-related diseases.

Materials and methods

Ethics statement

Animals were deeply anaesthetized with ether and decapitated, procedure authorized by the University of Chile Ethics Committee in accordance to EU Council Directive 86/609/EEC of 24 November 1986.

Brain slices

Fourteen-to-20-day-old Sprague–Dawley rats were deeply anaesthetized with ether and decapitated. The brain was rapidly removed and placed in ice-cold dissection artificial cerebrospinal fluid (ACSF) containing (in mM): NaCl, 124; KCl, 3; $NaHCO_3$, 26; NaH_2PO_4, 2.5; $CaCl_2$, 1; $MgSO_4$, 3; glucose, 10. This solution was equilibrated with a mixture of 95% O_2 and 5% CO_2 to obtain a final pH of 7.4. The brain was hemisected, and the cut surface glued to the stage of a vibratome (Campden Instruments, Loughborough, UK) with cyanoacrylate adhesive. The cutting chamber was surrounded with ice-cold ACSF and slices were cut in the dorso-inferior direction in the 45° plane to a thickness of 300/400 μm. Slices were then placed in a holding chamber and incubated at 34 °C for 1 h in ACSF before starting recordings. The slices were transferred to a recording chamber, where they were superfused with ACSF at 30–34 °C. The standard recording ACSF has the following composition (in mM): NaCl, 124; KCl, 2.5; $NaHCO_3$, 26; NaH_2PO_4, 2.5; $CaCl_2$, 2; $MgSO_4$, 2; glucose, 10. Experiments shown in Fig. 10 were performed with modified ACSF, used to generate extra network activity, where the concentration of the following chemicals was altered (in mM): KCl, 3.5; $CaCl_2$, 1.2; $MgSO_4$, 1. Standard and modified ACSF had less than 1.6 nM copper, measured on a Bruker S2 PICOFOX total reflection X-ray fluorescence spectrometer with a 0.1 ppb resolution.

Extracellular recordings

Extracellular recording of APs from the hippocampus CA1 pyramidal layer were performed in acute brain slices using tungsten microelectrodes (4–6 Mohms; FHC). A glass microelectrode, filled with standard recording ACSF, was used to record field postsynaptic potentials on the stratum radiatum. Signals from microelectrodes were amplified (× 10 000) and band-pass-filtered at 0.3–1 kHz with an A–M system amplifier (DA 1800). ACSF-filled glass electrodes, 2–5 Mohms, or bipolar tungsten stimulating electrodes were placed in the stratum radiatum of the hippocampus CA3 region to stimulate Schaffer collaterals.

Intracellular recordings and stimulation

Whole-cell current-clamp recordings were performed in the bridge balance mode with an AxoPatch 200B patch-clamp amplifier (www.moleculardevices.com). Patch-clamp microelectrodes were formed in a P-87 Flaming/Brown micropipette puller (www.sutter.com) to obtain 3–5 Mohm pipettes when filled with the intracellular solution containing (in mM): K-gluconate, 100; KCl, 20; Mg-ATP, 4; GTP, 0.3; HEPES, 10; phosphocreatine, 10; and titrated to pH 7.3 using 0.5 N KOH/KCl. Pyramidal neurons were observed and identified with IR-DIC optics under a 40× objective of a Nikon Eclipse E600FN microscope. Giga-seal and whole-cell recordings were performed under current-clamp as described (Hamill *et al.*, 1981). The intensities of the near-threshold depolarizing current ramps were adjusted for each cell. Supra-threshold intensity was 2× or 3× the near-threshold intensity; the same stimulation waveforms were used for simulation in experiments and simulations. The AP voltage threshold (V_{th}) was operationally defined as the membrane potential at which V_m depolarizes at the rate of 15 V/s (Kole *et al.*, 2008; Hu *et al.*, 2009).

Data acquisition, analysis and modelling

Data were analogue filtered at 1 or 5 kHz, digitized at 10 kHz and 12 bits resolution. Offline analysis was performed using Igor Pro (v5.0, www.WaveMetrics.com) with custom-made routines and Neuromatic v1.9-2.0 (www.ThinkRandom.com). Spontaneous excitatory postsynaptic currents (EPSCs) or spikes were detected using two-threshold detection routines. Threshold levels were set to the average ± twice the root mean square noise level, estimated for every recording during periods without activity. To allow copper diffusion, its effects were assessed by measuring neuronal activity 5 min after replacement of the control solution with copper-containing solution. Raster plots for every condition were performed to display event time sequences either for spikes or EPSCs; inter-event interval histograms and peri-stimulus time histograms were also analysed. Event frequencies were estimated by averaging the number of spikes or EPSCs detected in 1-s epochs. Time-to-first-spike after Schaffer collaterals' stimulation was taken as the average time to the first spike from a group of 5–10 repetitions of the same stimulation intensity. Synaptic transmission stability was evaluated by low-frequency stimulation (LFS; 0.33 Hz) during 300 s. Data are presented as average ± SEM. Statistical significance was evaluated to a significance level of 0.05 and assessed as indicated in the text. Spike classification was performed offline using wavelet analysis (Letelier & Weber, 2000). Membrane potential fluctuation experiments were performed in somatic whole-cell current-clamp configuration. Frozen noise currents were synthesized by arithmetical addition of near-threshold (1×) or supra-threshold (2× or 3×) direct current plus a Gaussian-distributed noise with a variance scaled for each cell. Neuronal modelling was performed in the NEURON simulation environment (www.neuron.yale.edu). Kinetics acceleration was implemented by scaling m and h time constants of axonal or somatic sodium channels.

Reliability and jitter analysis

Reliability analysis was performed for N successive AP sequences evoked by frozen noise current injections and computed by the correlation method (Schreiber *et al.*, 2003). To represent the N spike trains as vectors, $\vec{S}_i(i = 1, \ldots, N)$, they were convolved with a boxcar filter of 1 ms. Pairwise correlation was evaluated by computing

the scalar product of each vector pair. Reliability, R_{corr}, was computed as the mean of these normalized scalar products according to the following formula (Schreiber *et al.*, 2003)

$$R_{\mathrm{corr}} = \frac{2}{N(N-1)} \sum_{i=1}^{i=N} \sum_{j=i+1}^{j=N} \frac{\vec{S}_i \cdot \vec{S}_j}{|s_i||s_j|}$$

The normalization guarantees that $R_{corr} \in [0; 1]$. $R_{corr} = 1$ indicates the highest reliability and $R_{corr} = 0$ the lowest. To address the effect of copper on APs' reliability apart from its correlated effect on excitability, a 'masked train' was produced by masking out the extra spikes (see 'Mask' in Fig. 4B). Thus, the APs remaining in masked trains were used to calculate a 'Masked-reliability' that better captures changes in reliability induced by copper. Equivalent AP isochronous groups were defined as spikes occurring within 5-ms time windows. Jitter was calculated for each spike in the group as the time difference from the average. Cumulative distribution density function was calculated for all groups and averaged across experiments.

Copper concentration

Bathing solution copper concentrations are reported for each experimental condition. No attempt was made to calculate the actual copper concentration on the tissue. To reduce copper concentration nominally to zero, 20 μM of the non-toxic, copper-specific chelating agent, bathocuproinedisulphonic acid (disodium salt; BCP) was used with a BCP-Cu^{2+} dissociation constant (K_d) $\approx 10^{-20}$ (Xiao *et al.*, 2011).

Chemicals

All chemicals were from either Sigma-Aldrich (St Louis, MO, USA) or Merck (Darmstadt, Germany). Concentrated copper (as $CuCl_2$) stock solutions were prepared on a daily basis.

Results

How do small changes in sodium channel kinetics alter excitability of CA1 cells? – a computer simulation

Nanomolar copper accelerates activation of sodium channels and inactivation kinetics, and induces a higher spontaneous discharge frequency in frog olfactory neurons (Delgado *et al.*, 2006; Aedo *et al.*, 2007) To investigate the effects of small changes in sodium channel kinetics for neurons having typical pyramidal morphology, a computational model was used that considers neuron geometry and standard Hodgkin–Huxley kinetics (Kole *et al.*, 2008; Fig. 1A, inset). The model behaviour was explored using two stimulation protocols: a depolarizing current ramp protocol (34 mV/s; Fig. 1A); and frozen noise current injections (see Materials and methods; noise superimposed in a DC level, bottom trace Fig. 1B). The effect of 5 and 10% increases on the activation and inactivation time constants of axonal sodium channels on the generation of somatic APs was evaluated. An increased excitability was found, revealed either by the shorter delay for the AP generation during the ramp stimulus or by the increased discharge rate for random stimuli. This can be seen as a decrease in the AP initiation delays indicated by arrows and the raster above the spike trains in Fig. 1A and B, respectively. Quantitative evaluation reveals an increase in the amplitude and a decrease of rising time for APs induced by both protocols (Fig. 1C). AP amplitude displays a significant difference for 5 and 10% acceleration vs. control ($P \leq 0.05$, Kruskal–Wallis and stands for Nonparametric Multiple Comparison (NPMC) test). The average AP amplitude in mV was as follows: control, 64.2 ± 0.6, $n = 38$; 5%, 69.0 ± 0.4, $n = 45$; 10%, 72.8 ± 0.4, $n = 52$. AP rise time (10–90% amplitude) is significantly shorter ($P \leq 0.05$, one-way ANOVA and Dunnett test). The average rise time for the control group (in ms) was 0.306 ± 0.003 ($n = 38$), whereas that reached 0.277 ± 0.002 ($n = 45$) and 0.256 ± 0.002 ($n = 52$) for 5 and 10% acceleration, respectively. An additional finding is that the acceleration of sodium channel kinetics shortens the AP half-width and lowers AP threshold. Five percent acceleration in sodium channel kinetics induced a 3% shortening of AP width, while 10% acceleration produced a 6% shortening (Fig. 1D). Ten percent acceleration hyperpolarized V_{th} by 2 mV, while 5% acceleration produced almost half this effect (Fig. 1E, left panel). Furthermore, V_{th} hyperpolarization depends on whether axonal initial segment (AIS) or somatic sodium channel kinetics are accelerated. The percent change of V_{th} caused by acceleration of AIS sodium channels kinetics is three times larger than the corresponding change for somatic channels, as shown in Fig. 1E. Simulations indicate that the high density of sodium channels located in AIS controls AP initiations by setting V_{th}. Also, the AP discharge rate is modulated by sodium channel kinetics (Fig. 1F), but interestingly the gain of the frequency–intensity (*f–I*) transfer function remains unchanged (Fig. 1G). Based on these simulations and the previous results in olfactory neurons (Delgado *et al.*, 2006), it was proposed that copper modulates neuronal excitability on central neurons by accelerating sodium channel kinetics at the axon initial segment.

Copper lowers AP threshold and accelerates the repolarization phase on CA1 neurons

Based on the results of neuronal simulations, the copper effects on V_{th} and AP half-width on CA1 neurons of rat acute hippocampal slices were investigated under whole-cell recording in response to the same stimulation protocols used in the simulations: a slowly depolarizing ramp (current adjusted to result in a voltage ramp of 34.1 ± 2.7 mV/s; $n = 8$) and near- or supra-threshold frozen noise current injections. Figure 2A shows AP trains induced by either ramp injections (top) or near-threshold frozen noise current injections (bottom) to a pyramidal CA1 neuron in the absence (control) and under 50 and 100 nM copper. Qualitative examination of raw traces under either stimulation conditions reveals that copper increases spiking frequency. AP profiles alignment at the times of reaching V_{th}, obtained either from ramp stimulation (upper traces) or from frozen noise current injections (lower traces), reveals the repolarization phase is faster, therefore the AP width decreases as expected from model simulations (Fig. 2B and C). A quantitative analysis reveals that V_{th} becomes significantly more negative in the presence of copper for all stimulation protocols (Fig. 2D). The average V_{th} values for the ramp stimulating protocol in control conditions were significantly depolarized compared with 50 and 100 nM Cu^{2+} (−49.4 ± 0.9 mV, $n = 8$; −51.1 ± 0.9 mV, $n = 8$; −52.7 ± 1.1 mV, $n = 6$; control, 50 nM, 100 nM Cu^{2+}, respectively, $P \leq 0.05$, Kruskal–Wallis test). Similarly, APs evoked by the frozen noise protocol had V_{th} values 1.5–3.0 mV more hyperpolarized by 50 and 100 nM Cu^{2+} in comparison with control either for near-threshold or supra-threshold stimulation (Fig. 2D; $P \leq 0.05$, Kruskal–Wallis test). AP duration was evaluated by measuring AP half-width for both stimulation protocols. In both experimental conditions copper causes a significant decrease on this parameter, as shown in Table 1 ($P \leq 0.05$, Kruskal–Wallis test). However, no sig-

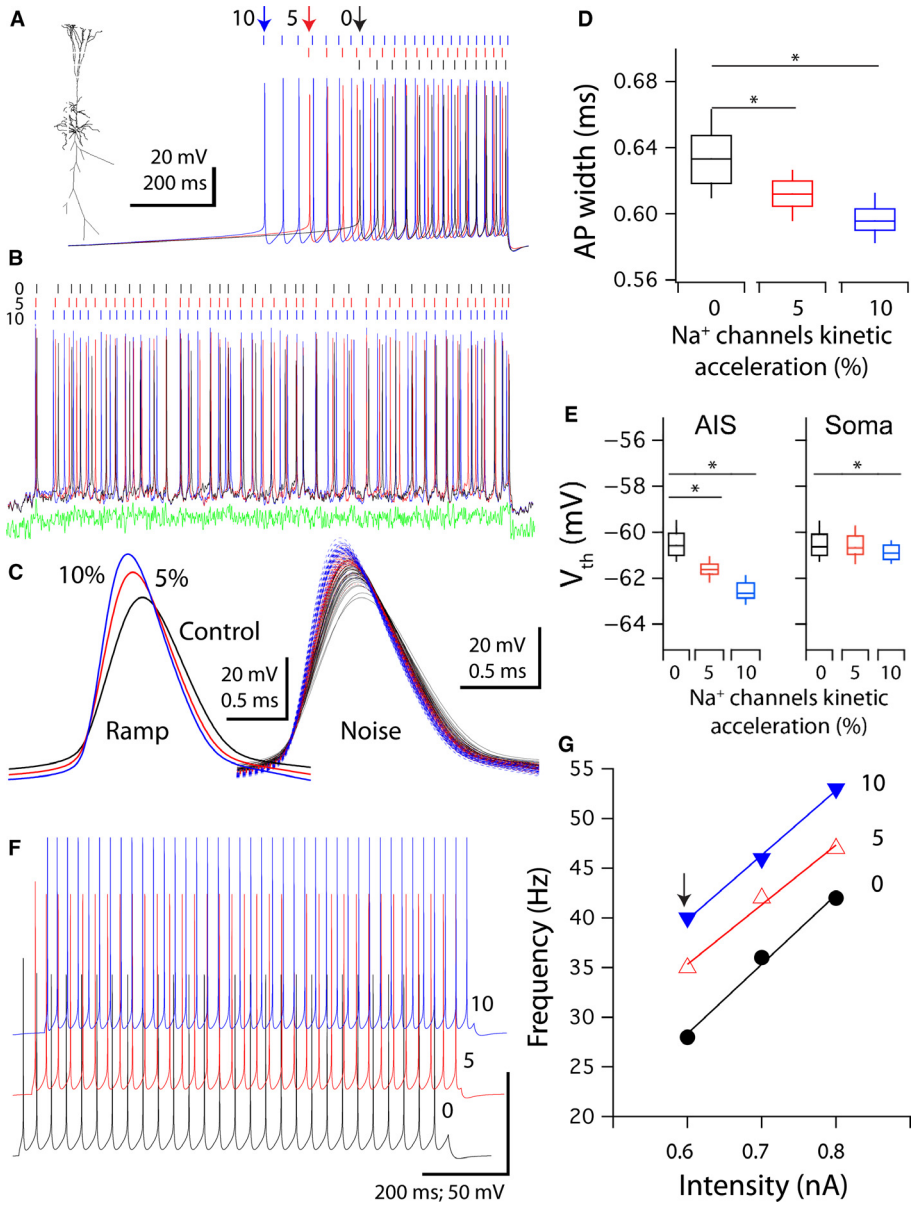

FIG. 1. Effects of sodium channel kinetics acceleration in a pyramidal neuron model. (A) Simulated somatic action potential (AP) obtained by depolarizing current ramp injections, for the case of 0% (control), 5 and 10% increases in acceleration of axonal sodium channels (inset = morphology of the neuronal model used). (B) Simulated AP trains were obtained by near-threshold frozen noise current stimuli. The model generates higher discharge rates as the sodium channel kinetics acceleration increases from 0% (38 APs) to 5% (45 APs) and to 10% (52 APs). (C) AP profiles, for ramp (left traces) and frozen noise (right traces) simulated responses. (D) Box-plot of AP duration values for 0, 5 and 10% acceleration for noise triggered APs shown in (B). AP width (ms): 0.645 ± 0.003 (n = 38); 0.613 ± 0.002 (n = 45); 0.598 ± 0.002 (n = 52); control, 5 and 10% acceleration, respectively. (E) Somatic V_{th} values obtained by sodium channels activation/inactivation kinetics acceleration at the axonal initial segment (AIS) vs. soma. (F) Axonal sodium channel acceleration increases discharge rate for DC stepped stimulation: 0 (control), 5 and 10%. (G) Simulated *f–I* transfer function obtained by axonal sodium channel acceleration as indicated (arrow = data shown in F). *indicates statistical significance evaluated to a significance level of $P \leq 0.05$.

nificant changes in AP amplitude or membrane input resistance were observed (Fig. 2C; Table 1). These results suggest that copper modulates neuronal excitability by accelerating sodium channel kinetics resulting in lowering V_{th} levels by 2 or 3 mV, and AP duration by 12–14%, as was demonstrated from the model simulation.

Copper maintains gain, but changes the offset of the neuronal input–output transfer frequency–intensity (f–I) function

As in the simulations on the neuron model the slope of the *f–I* curve was not affected by changes in sodium channel kinetics, it was then examined if copper affected the *f–I* response using near (1×) and supra-threshold (2×, 3×) DC-stepped stimulation (Fig. 3). For near-threshold stimulation, copper regularizes the temporal pattern of evoked trains of APs as revealed by the low variability between successive trains [Fig. 3A, 15 superimposed successive traces under 0 (control), 50 and 100 nM added copper]. A similar regularization is also observed in the absence of copper but for supra-threshold stimulation (Fig. 3B, 2× and 3× traces). In the presence of copper the supra-threshold behaviour can be reached for weaker near-threshold stimulation; we suggest that a target of copper might be the membrane dynamics biophysics responsible for AP generation, i.e. near-threshold V_m regime. Next it was evaluated how copper modulates the rate of AP generation by measuring the (*f–I*) transfer function at

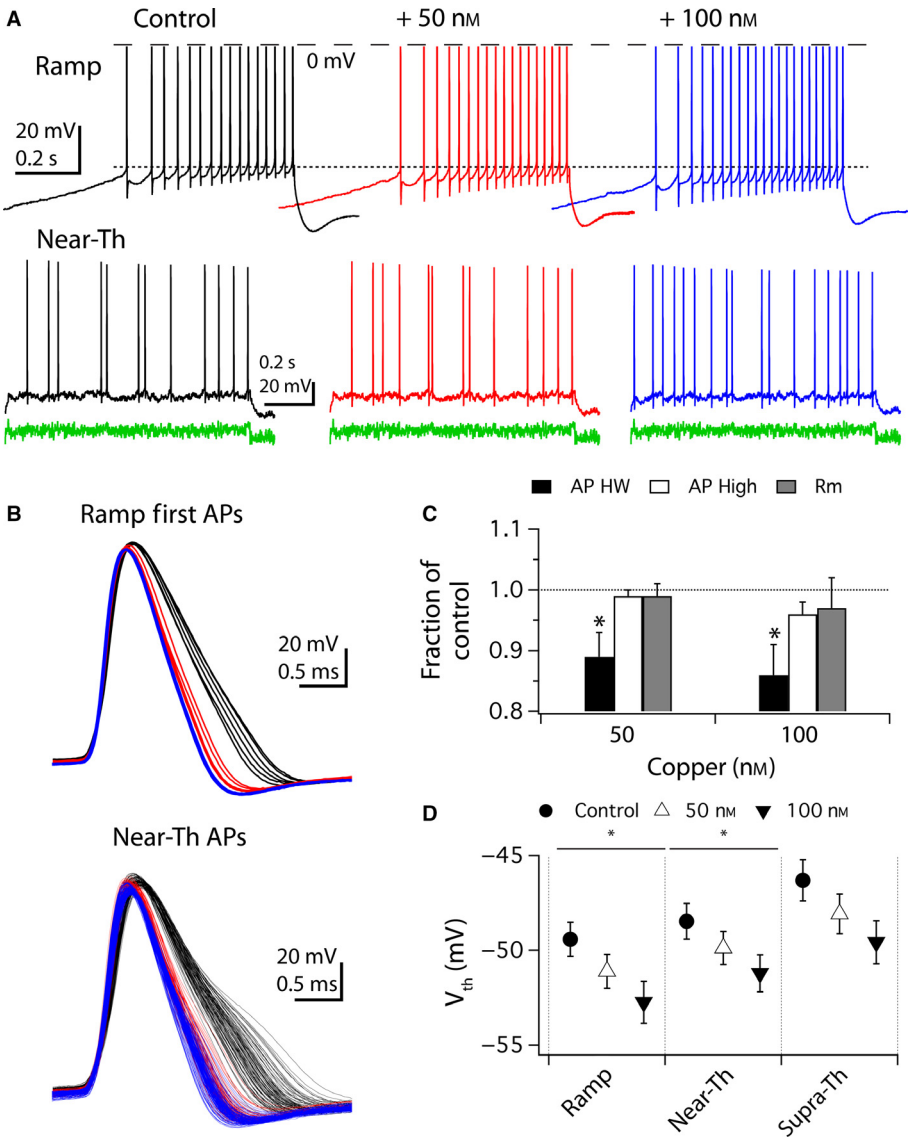

FIG. 2. Effects of nanomolar copper concentration on CA1 neurons. (A) Neuronal V_m traces under whole-cell current-clamp obtained in control and after bath-application of 50 and 100 nM Cu^{2+}. V_m records obtained for ramp stimulation (upper panel), dotted line indicates V_{th} value for the first action potential (AP); and records obtained for near-threshold frozen noise current injections (lower panel, Near-Th). (B) AP profiles triggered by current ramp (upper panel) and near-threshold stimulations (lower panel). (C) Quantification of copper effect on AP parameters. AP half-width [AP HW (ms) ramps, 0.92 ± 0.04, n = 8; 0.81 ± 0.03, n = 8; 0.77 ± 0.02, n = 6; control, 50 and 100 nM copper; noise, 0.93 ± 0.05, n = 8; 0.81 ± 0.03, n = 8; 0.76 ± 0.02, n = 6; control, 50 and 100 nM copper], AP amplitude [AP high (mV): 89.8 ± 7.8, n = 8; 88.8 ± 8.1, n = 8; 88.0 ± 8.7, n = 6; control, 50 and 100 nM copper] and membrane input resistance [R_m (as fraction of control): 0.92 ± 0.05, n = 8; 0.93 ± 0.06, n = 6; 50 and 100 nM copper, respectively] for near-threshold frozen noise and ramp-series under 50 and 100 nM Cu^{2+}, see Table 1. (D) Somatic V_{th} quantification, for ramps: −49.4 ± 0.9 mV, n = 8; −51.1 ± 0.9 mV, n = 8; −53.3 ± 0.9 mV, n = 6 (control, 50, 100 nM Cu^{2+}, respectively), near-threshold: −47.7 ± 0.9 mV, n = 6; −51.0 ± 0.4 mV, n = 6; −51.2 ± 0.8 mV, n = 6 (control, 50, 100 nM Cu^{2+}, respectively) and supra-threshold: −45.4 ± 1.0 mV, n = 6; −49.5 ± 0.5 mV, n = 6; −49.6 ± 0.9 mV, n = 6 (control, 50, 100 nM Cu^{2+}, respectively) stimulating conditions. There is a linear relationship between V_{th} and copper concentration (0.035 ± 0.001 mV/nM, r^2 = 0.99). *indicates statistical significance evaluated to a significance level of $P \leq 0.05$.

two different copper concentrations. Figure 3C summarizes how copper increases discharge rates in near (1×) and supra-threshold (2× and 3×) conditions. Interestingly, the changes induced by copper upon the (*f–I*) transfer function act in a very specific manner, as they are independent of stimulus intensity. Therefore copper, as predicted in the model (Fig. 1G), does not affect the slope of the *f–I* relationship transfer function [control: 11.8 ± 1.0, n = 8; 50 nM Cu^{2+}: 12.7 ± 1.3, n = 8; 100 nM Cu^{2+}: 12.2 ± 1.7, n = 6 (Hz/unitary stim. intensity); $P > 0.05$ Kruskal–Wallis test], but does change its offset (7.37 ± 1.56, n = 8; 11.50 ± 0.96, n = 8; 15.00 ± 2.56, n = 6; Hz at 1× stimulation intensity, control, 50 and 100 nM Cu^{2+}, respectively; $P \leq 0.05$ ANCOVA test). In summary, these results show that copper enhances excitability at the single cell level generating more AP, while maintaining (*f–I*) transfer function gain invariant. These results are consistent with the notion that copper accelerates the sodium channel kinetics, as observed in the neuron simulations (Fig. 1).

Time processing and spike reliability in CA1 cells

In order to test if the regularization of the spike firing pattern induced by copper (Fig. 3A) also improves the reproducibility of

TABLE 1. Cell and action potential parameters

	Control	50 nM	100 nM
AP half-width (ms) ramp protocol	0.92 ± 0.04 (n = 8)	0.85 ± 0.03 (n = 8)	0.77 ± 0.03 (n = 6)
AP half-width (ms) frozen noise injection	0.93 ± 0.05 (n = 8)	0.81 ± 0.03 (n = 8)	0.77 ± 0.02 (n = 6)
AP amplitude (mV) frozen noise injection	89.8 ± 7.9 (n = 8)	88.9 ± 8.1 (n = 8)	88.0 ± 8.7 (n = 6)
R_m (fraction of control) frozen noise injection	1.00 ± 0.06 (n = 8)	0.99 ± 0.02 (n = 8)	0.97 ± 0.05 (n = 6)

AP, action potential; Rm, membrane resistance.

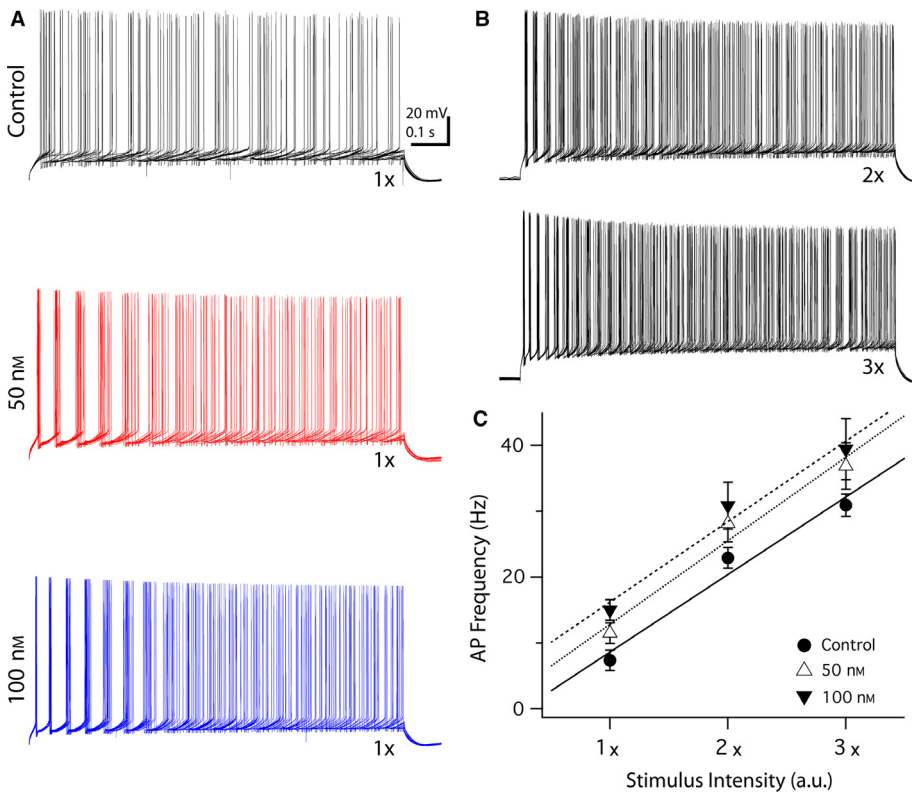

FIG. 3. Copper effects on *f–I* transfer function of CA1 neurons. (A) Fifteen superimposed whole-cell action potential (AP) train recordings induced by DC-stepped depolarizations under control, 50 nM (middle) and 100 nM (lower) Cu^{2+} for near-threshold stimulation (1×). (B) Spiking activity patterns for supra-threshold stimulation (2×, 3×) with no added Cu^{2+}. (C) *f–I* transfer function at control, 50 and 100 nM added Cu^{2+}. Linear regression of discharge rate vs. stimulus intensity shows a significant difference in the offset parameter but no significant differences in the slope (r^2 = 0.98).

evoked spike trains produced by identical stimuli, the correlation-based measure of spike timing reliability, R_{corr} (see Materials and methods; Schreiber *et al.*, 2003), was used. Figure 4A displays two spike trains obtained in control and 50 nM Cu^{2+}, induced by frozen noise current injections in the near-threshold condition under whole-cell current-clamp. Similar AP trains were evoked in both cases but, due to the higher excitability induced by copper, a few extra APs were visible (indicated by arrows). Ten–twenty repetitions for control and experimental conditions were recorded. Raster diagrams of those repetitions show the degree of variability of the time of spike occurrence for both conditions (Fig. 4B). R_{corr} was quantified for control and copper before and after masking out the extra spikes (see Materials and methods). A significant improvement in AP reliability induced by copper for either all the APs recorded in the presence of copper ('All AP' column) or only the masked APs ('Masked AP' column; Fig. 4C) was observed. Notably, this increase in reliability only occurs for near-threshold stimulation ($P \leq 0.05$, Wilcoxon signed rank test); supra-threshold conditions do not show significant changes in reliability of AP trains (Fig. 4C, bottom). This result indicates that improved reliability is directly related to a decrease in threshold, V_{th}, and not just a consequence of the increase in excitability produced by copper. Improved reliability occurs without noticeable changes in the jitter of timing of APs, as shown by the cumulative density function of APs lags (Fig. 4D). As expected, 50 and 100 nM Cu^{2+} significantly increase AP frequency induced by frozen noise stimulation either for near- or supra-threshold level (Fig. 4E; $P \leq 0.05$, Kruskal–Wallis test). Interestingly, these results indicate that copper modulates V_m near-threshold allowing an improved reliability at the same time that allows higher AP frequency.

Copper increases the frequency of spontaneous postsynaptic events in CA1 pyramidal cells

The previous results indicate that copper modulates key biophysical steps leading to increased excitability at the single cell level. To evaluate if this increased excitability also impacts onto network activity, the effects of copper were quantified at nanomolar concen-

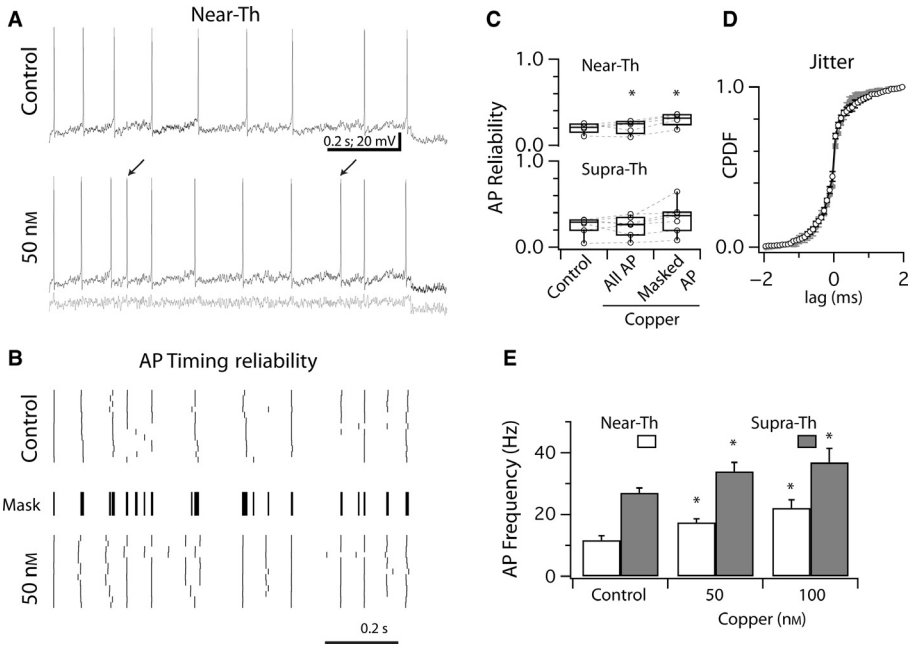

FIG. 4. Nanomolar Cu^{2+} improves action potential (AP) timing reliability. (A) AP trains induced by frozen noise current injections in control condition (upper trace), and under 50 nM Cu^{2+} (lower trace), extra spikes are indicated by arrows. The current stimulus is indicated under the AP trace in grey. (B) Raster plots of AP trains (n = 15) elicited by frozen noise current injections in control conditions and under 50 nM Cu^{2+}. (C) Box-plots representing AP timing pattern reliability in control conditions (control: 0.23 ± 0.05, n = 7), 50 nM copper (All AP: 0.26 ± 0.06, n = 7; Masked AP: 0.37 ± 0.04, n = 7) for near-threshold. Supra-threshold stimulation: control (0.29 ± 0.03, n = 7), 50 nM copper (All AP: 0.27 ± 0.03, n = 7; Masked AP: 0.37 ± 0.06, n = 7). (D) AP jitter data presented as a cumulative density probability distribution in control (open circles) and in the presence of 50 nM Cu^{2+} (grey symbols). (E) AP frequency induced by frozen noise current injections for near-threshold and supra-threshold stimulation in control, 50 and 100 nM Cu^{2+} conditions (near-threshold in Hz: 11.7 ± 1.4, n = 8; 17.4 ± 1.2, n = 8; 22.1 ± 2.3, n = 6, control; 50 nM; 100 nM; supra-threshold: 27.1 ± 1.6, n = 8; 34.0 ± 2.9, n = 8; 36.9 ± 3.3, n = 8, control; 50 nM; 100 nM). AP frequency increases at a rate of 1% per nanomolar copper concentration increase. *indicates statistical significance evaluated to a significance level of $P \leq 0.05$.

tration upon the frequency of synaptic events reaching CA1 pyramidal neurons. EPSCs elicited by the spontaneous network presynaptic activity arriving to CA1 pyramidal neurons under voltage-clamp were recorded. Figure 5A displays spontaneous EPSCs (left panels) and their raster plot representation (right panels). The excitatory postsynaptic events frequency increased from 2.90 ± 0.62 events/s (n = 23) in control condition to 4.33 ± 0.68 events/s (n = 33) in the presence of 50 nM copper (control vs. copper, $P < 0.05$ one-tailed t-test). The average frequency of EPSC rose by 44 ± 10% (n = 21) and 82 ± 33% (n = 12) after exposure to 50 and 100 nM Cu^{2+}, respectively (Fig. 5B). The EPSC frequency is significantly higher in the presence of copper; nevertheless, there is no statistical difference between the two different copper concentrations (one-way ANOVA). Copper-triggered increases in EPSC frequency are not observed in the presence of tetrodotoxin (TTX; two-way ANOVA, $P < 0.05$; Fig. 5C), while amplitudes of EPSCs were not significantly different from control, as determined by the amplitude distribution (Fig. 5D) or the cumulative density function for amplitudes (Fig. 5E; $P > 0.05$ Kolmogorov–Smirnoff test). Therefore, copper increases the frequency of TTX-sensitive EPSCs.

Copper enhances the variability of the CA1 response to CA3 stimulation

To evaluate whether copper influences Schaffer projections to CA1, the input–output relationship to CA1 neurons was quantified by comparing the slope of the evoked field excitatory postsynaptic potential (fEPSP) related to the fibre volley amplitude in response to increasing stimulus strength delivered to Schaffer collaterals in control conditions, and after adding 10, 50 and 100 nM Cu^{2+} to the slices (Fig. 6). In order to evaluate synaptic transmission stability, fEPSPs were recorded during 5 min of LFS (0.33 Hz). The upper left panel in Fig. 6A shows 100 superimposed fEPSP repetitions recorded in control conditions. The bottom plots show the summary time course for the relative volley and slopes of fEPSP-evoked response. After a stable baseline recording, the input/output relationship was evaluated by 5–10 repetitions at increasing intensities of stimulation (upper right panel). As the stimulus amplitude increases, more presynaptic fibres are recruited and the presynaptic volley amplitude increases accordingly (see arrows in Fig. 6A). As more fibres are recruited, more neurotransmitter was released and the fEPSP amplitude also increased. Figure 6B shows the normalized fEPSP slopes vs. the normalized volley amplitude obtained in different control experiments. The same layout is used for displaying data in the presence of 10, 50 and 100 nM copper concentration (Fig. 6C–H). The statistical analysis of variance considering each concentration does not show significant differences in the average relative slopes (1.00 ± 0.02, 1.52 ± 0.45, 1.07 ± 0.13, 1.14 ± 0.16, for control, 10, 50 and 100 nM Cu^{2+}, respectively; Kruskal–Wallis test, P = 0.80). However, as is seen in Fig. 6, the input/output relationship becomes more variable along all copper concentration used (CV 0.08, 0.67, 0.43, 0.40 for control, 10, 50 and 100 nM copper, respectively), indicating a higher heterogeneity of the activated synapses in the presence of nanomolar copper. As a consequence, copper can effectively modify the CA3 → CA1 pathway on the hippocampus network.

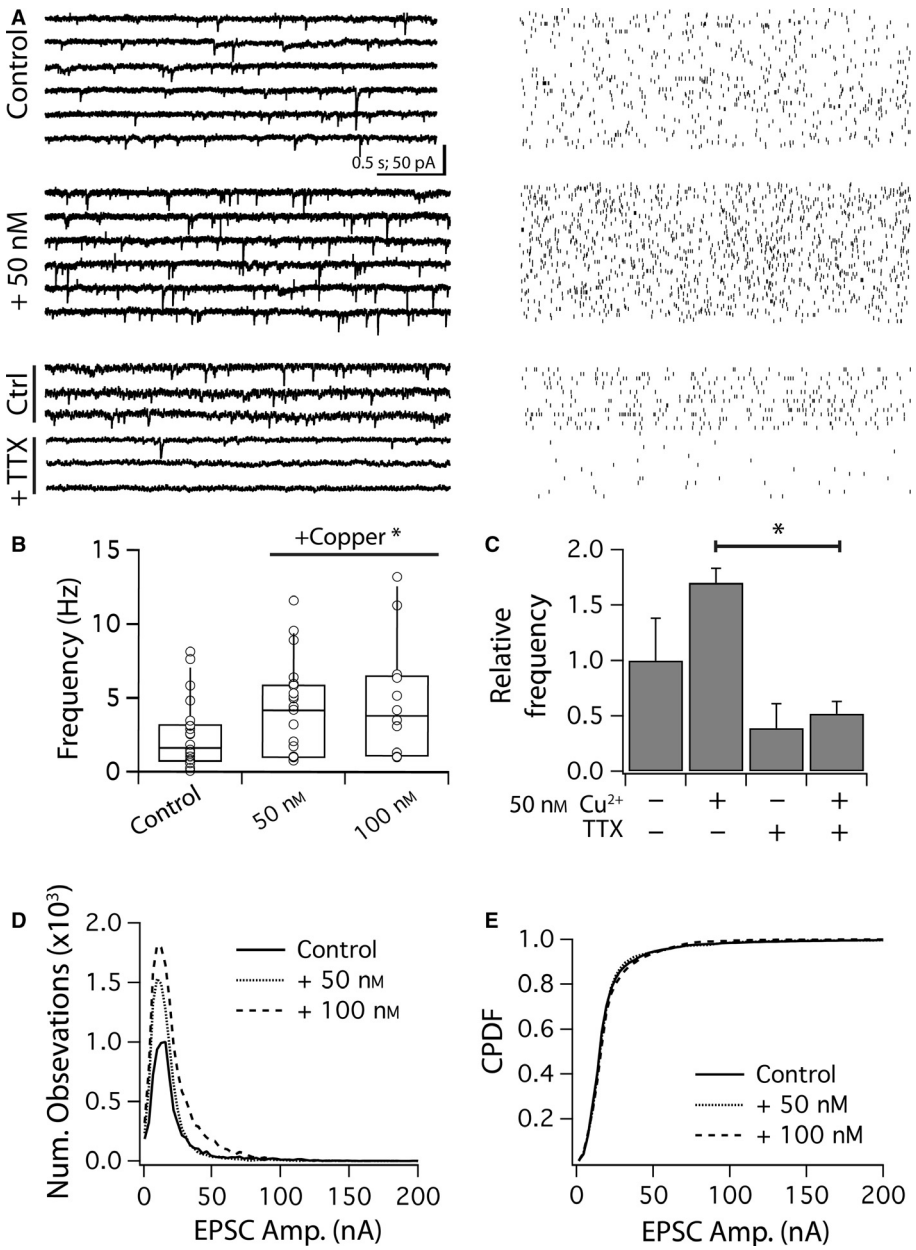

FIG. 5. Copper increases the frequency of spontaneous excitatory postsynaptic currents (EPSCs) in CA1 principal cells. (A) Left panels display whole-cell voltage-clamp (−70 mV) recordings; in control (upper traces) and under 50 nM Cu^{2+} (middle traces), and in control and tetrodotoxin (TTX; bottom traces) Right panels display raster plots of spontaneous EPSCs in each condition. (B) Box-plot quantification of frequency of EPSCs for control condition, 50 and 100 nM Cu^{2+} (in Hz: 2.90 ± 0.62, n = 23; 4.14 ± 0.70, n = 21; 4.82 ± 1.21, n = 12). Relative frequency change: 1.43 ± 0.09, n = 21; 1.82 ± 0.27, n = 12 for 50 and 100 nM Cu^{2+}, respectively (Kruskal–Wallis test, $P < 0.05$). (C) Relative change of frequency of spontaneous EPSCs induced by 50 nM Cu^{2+} and its dependence on TTX-sensitive channels (two-way ANOVA, $P < 0.05$). (D) Amplitude distribution of EPSCs in control, 50 and 100 nM Cu^{2+}. (E) Cumulative probability density function for amplitudes of EPSCs. *indicates statistical significance evaluated to a significance level of $P \leq 0.05$.

Calcium-dependent short-term plasticity is unaffected by copper

It was questioned whether copper affects calcium-dependent short-term plasticity. This type of plasticity was evaluated by measuring the ratio of the slopes of the fEPSPs triggered under paired-pulse stimulation protocols on Schaffer collaterals. Synaptic facilitation by paired-pulses has been shown to follow the time course of calcium clearance on presynaptic terminals (Chen & Regehr, 1999; Dittman *et al.*, 2000; Zucker & Regehr, 2002). Figure 7A shows the result of a paired-pulse protocol where the interval between the control pulse (P) and a second test pulse (P_{test}) varied from 20 ms to 2 s. After paired-pulse stimulation, synaptic transmission increased by about 90% of the value prior to stimulation, therefore this protocol facilitates synaptic transmission (compare the recordings for the first and second fEPSP for the three conditions). The values for the paired-pulse fEPSP slope ratio in control and copper-treated slices were not significantly different. The paired-pulse fEPSP ratio rise-time course is fast as the maximum occurs within the first 20 ms. Facilitation reaches a maximum and relaxes exponentially in < 1 s. No significant differences were found in the decay time constant or magnitude of facilitation for the control and copper-exposed conditions (time constant in seconds, control: 0.50 ± 0.16, n = 7; Cu^{2+}

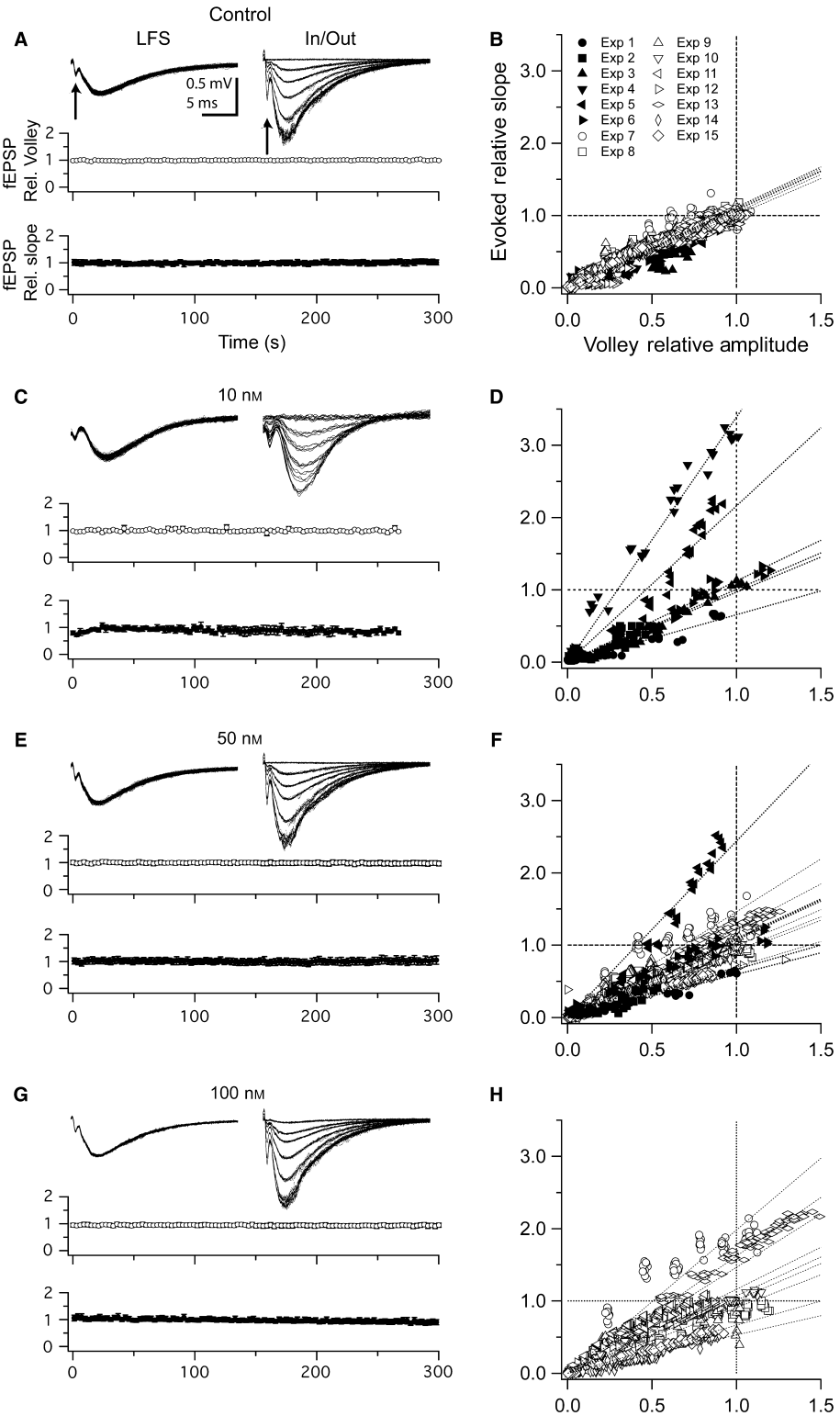

FIG. 6. Copper increases the variability of the input/output transfer function of the CA3 → CA1 pathway. (A, C, E, G) Graphs: standardized volley amplitude (upper plot) and standardized slopes (lower plot) of field excitatory postsynaptic potentials (fEPSPs) obtained at constant intensity and low-frequency stimulation regime (LFS, 0.3 Hz) in control condition and 10, 50 and 100 nM copper, obtained in representative experiments. LFS inset: 30–40 superimposed fEPSP recordings obtained during the LFS stimulation period. In/out inset, fEPSP recordings obtained for increasing stimulation intensities of Schaffer collaterals. Arrows indicate presynaptic volley. Average fEPSP slopes for LFS: 166 ± 21, 133 ± 33, 150 ± 25, 178 ± 28 (μV/ms), control, 10, 50 and 100 nM, respectively ($P > 0.05$, Kruskal–Wallis test, $n = 14, 5, 12, 9$, respectively). Average fEPSP volley amplitudes during LFS: 338 ± 63, 321 ± 73, 355 ± 94, 340 ± 118 (μV), control, 10, 50 and 100 nM, respectively ($P > 0.05$, Kruskal–Wallis test, $n = 14, 5, 12, 9$, respectively). (B, D, F, H) fEPSP slopes as a function of volley amplitude standardized to control conditions. Linear regressions are displayed for each experiment as dotted lines: 1.00 ± 0.02, 1.52 ± 0.45, 1.07 ± 0.13, 1.14 ± 0.16 ($n = 14, 5, 12$ and 9, respectively) relative slopes values for control, 10, 50 and 100 nM Cu^{2+}, respectively. Filled and open symbols correspond to data gathered at different times (1–6 older).

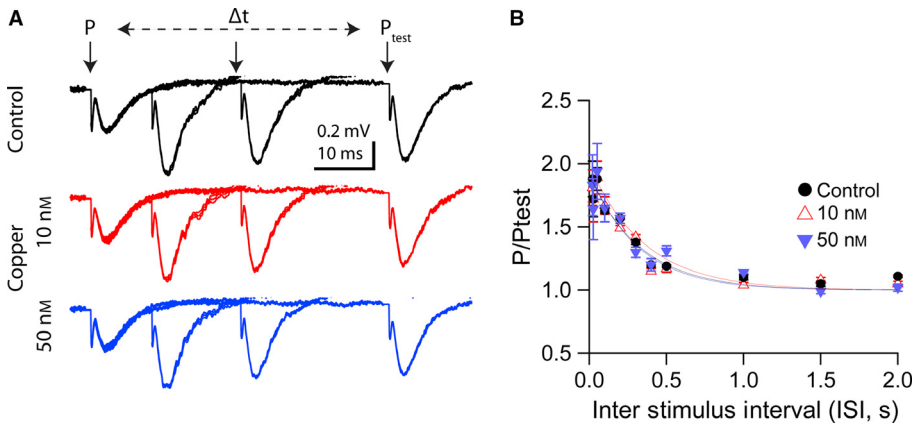

FIG. 7. Calcium-dependent short-term plasticity in CA3–CA1 synapses is unaffected by copper. (A) Evoked field potentials recording triggered by paired-pulse stimulation control (black), 10 nM copper and 50 nM copper for 20, 50 and 100 ms intervals. Paired-pulse stimulation was delivered at variable intervals (Δt between 20 and 2000 ms) to Schaffer collaterals with a fixed inter-pair stimulus (20 s). As expected, the response associated to the second pulse (P_{test}) is about twice the control pulse (P). (B) The (P_{test}/P) slopes ratio is shown as a function of the inter-pulse interval Δt. Individual experiments were fitted with an exponential function: 1 + Peak $e^{(-t/tau)}$. Average decay time constant parameter, tau in seconds, control: 0.50 ± 0.16, n = 7; Cu^{2+} 10 nM: 0.53 ± 0.18, n = 6; Cu^{2+} 50 nM: 0.57 ± 0.17, n = 5 (P = 0.86, Kruskal–Wallis test). Facilitation peak parameter: control: 0.91 ± 0.12, n = 7; Cu^{2+} 10 nM: 0.99 ± 0.14, n = 6; Cu^{2+} 50 nM: 0.93 ± 0.09, n = 5 (P = 0.98, Kruskal–Wallis test). Lines in the graph plot average fitting curves for each condition; similarly symbols represent average experimental values for each condition.

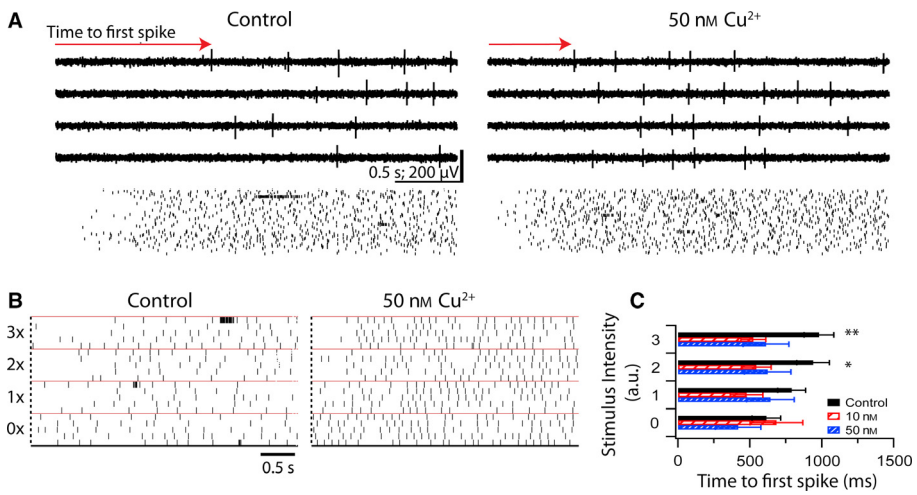

FIG. 8. Copper reduces feedforward inhibition. (A) Four traces, displaying CA1 spiking discharges recorded after Schaffer collaterals stimulation (1 μA, 1 ms) in control condition and under 50 nM copper in a representative experiment. Raster plots (below raw traces) display spiking activity for 90 repetitions for each condition. (B) Raster plots representing CA1 spiking discharges triggered by increasing stimulus intensities delivered to Schaffer collaterals, horizontal lines separate sets of five identical repetitions obtained with the same stimulus intensities 0× to 3×. (C) Quantification of the average time delay to first spike in control and the presence of 10 and 50 nM copper concentration (control: 0×: 614 ± 99; 1×: 790 ± 97; 2×: 939 ± 113; 3×: 980 ± 103 ms (n = 9); 10 nM copper: 0×: 684 ± 184; 1×: 477 ± 113; 2×: 544 ± 103; 3×: 524 ± 87 ms (n = 9); 50 nM copper: 0×: 418 ± 158; 1×: 642 ± 166; 2×: 623 ± 159; 3×: 612 ± 159 ms (n = 7; one-way ANOVA test: *P = 0.05, **P = 0.01).

10 nM: 0.53 ± 0.18, n = 6; Cu^{2+} 50 nM: 0.57 ± 0.17, n = 5, P = 0.86, Kruskal–Wallis test; facilitation peak, control: 0.91 ± 0.12, n = 7; Cu^{2+} 10 nM: 0.99 ± 0.14, n = 6; Cu^{2+} 50 nM: 0.93 ± 0.09, n = 5, P = 0.98, Kruskal–Wallis test). If copper would trigger differences in calcium clearance from the Schaffer terminals, changes of the decay time course of this process would be expected, but this was not observed (Fig. 7B). Therefore, copper does not affect presynaptic calcium levels or kinetics of short-term synaptic plasticity, suggesting that the variability in the input/output of fEPSP from CA3 to CA1 observed in the presence of copper (Fig. 6B, D and F) is related to a higher heterogeneity of activated synaptic contacts with similar short-term plasticity properties.

Copper overcomes CA1 feedforward inhibition

Copper inhibits $GABA_A$ receptors at nM concentrations (IC_{50} = 35 nM; Sharonova *et al.*, 1998, 2000), suggesting that copper might affect excitation/inhibition balance arriving to CA1 pyramidal neurons. Figure 8 shows that activation of Schaffer collaterals axons results in a transient silence of CA1 spiking activity, reflecting a perturbation in the excitation/inhibition balance. This silent period is shortened in the presence of 50 nM copper, consistent with a decrease on $GABA_A$-mediated inhibition. Figure 8A shows four extracellular recordings starting immediately after the stimulation pulse was delivered to Schaffer collaterals in control solution and in the presence of 50 nM copper; the raster plots below the traces summarize data from 90 such trials. Increasing stimulus intensity recruits

more excitatory and inhibitory components; a higher number of inhibitory components results in longer delays to first spike due to the time required to clear the GABA released by inhibitory neurons following the activation of Schaffer collaterals (Fig. 8B and C). The average time-to-first-spike values are 614 ± 99, 790 ± 97, 939 ± 113, 980 ± 103 ms (n = 9) for stimulus intensities 0×, 1×, 2×, 3×, respectively (Fig. 8C). These silent periods become shorter in the presence of 10 nM copper [684 ± 184, 477 ± 113, 544 ± 103, 524 ± 87 ms (n = 9)] and in the presence of 50 nM copper [418 ± 158, 642 ± 166, 623 ± 162, 612 ± 159 ms (n = 7, one-way ANOVA: $P \leq 0.05$). As shown in Fig. 6, copper does not change basal fEPSP upon Shaffer collaterals activation. Therefore, the change in excitation/inhibition balance revealed by the time to first spike is due to a decreased inhibition. Because this inhibition target is mediated by the feedforward inhibitory neurons, it is proposed that these cells are a target of copper.

Nanomolar copper enhances spontaneous AP firing rates in the CA1 region of the hippocampus

The previous results suggest a key influence of copper on neuronal excitability. To further investigate whether nanomolar Cu^{2+} concentrations modulate CA1 network excitability, spontaneous extracellular activity was quantified under control and 10 nM copper in CA1 area (Fig. 9A). The spontaneous frequency was significantly higher under copper (Fig. 9B and C), from 2.65 ± 0.33 to 3.74 ± 0.52 Hz (two-tailed Student's t-test, P = 0.0006, n = 38). Consistently, the cumulative probability density function for the frequency distribution displays a significant right-hand shift in the presence of copper, indicating an increase in spiking frequency (Fig. 9D; Kolgomorov–Smirnoff test, $P < 0.05$). To evaluate if the observed spiking activity enhancement was due to higher discharge rates of neurons already active during the control period, or alternatively to recruitment of new units, a copper sensitivity index (CSI) was defined as: number

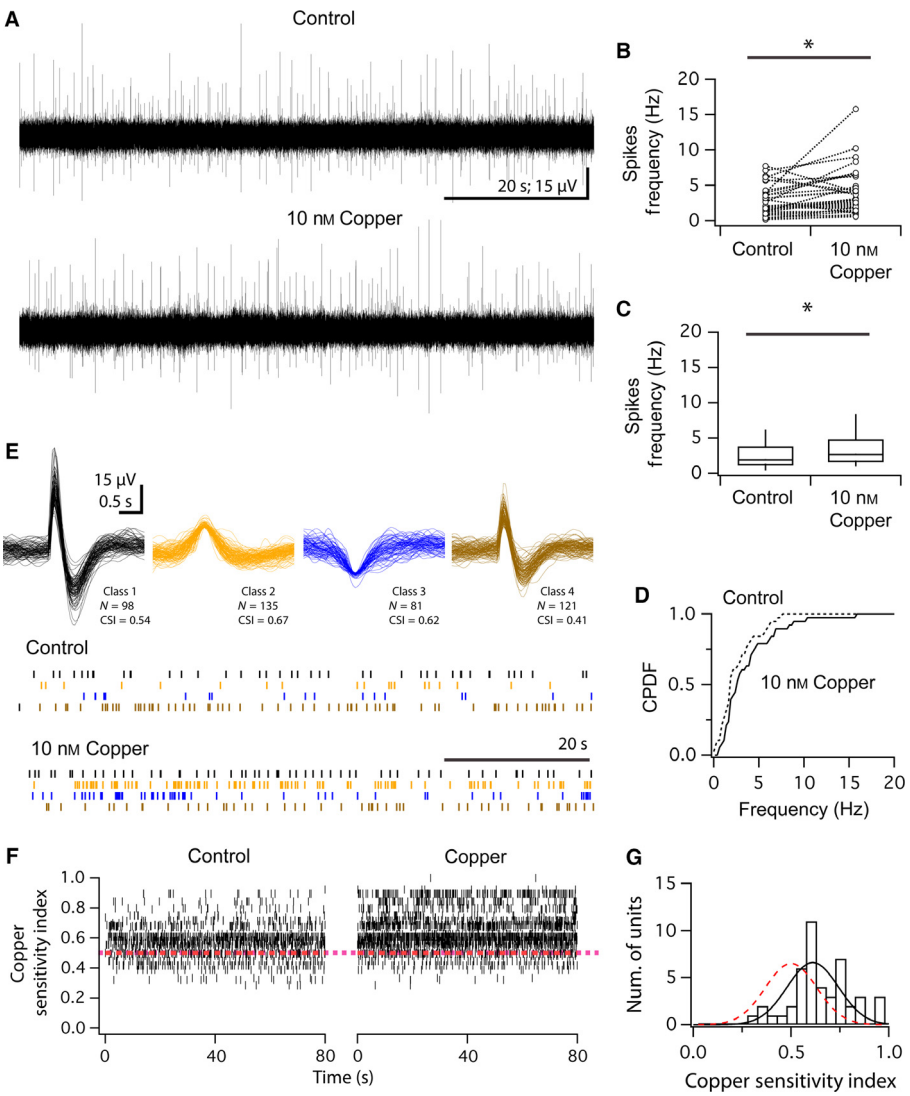

FIG. 9. Nanomolar copper increases spontaneous spike frequency in the CA1 region of the hippocampus. (A) Extracellular traces of spiking activity in control and after bath-application of 10 nM copper. (B) Paired data quantification of spontaneous multi-unitary activity from 38 experiments in control and under 10 nM copper. (C) Box-plot representation and (D) cumulative probability density function of the population data shown in (B). (E) Four spikes classes (units) of sorted spikes from the record shown in (A); activity patterns of the sorted spikes are shown as raster plots for both conditions Numbers indicate the total number of spikes for each class and its copper sensitivity index (CSI = number of spikes in copper)/[total number spikes (control + copper)]. (F) Raster representation of activity in 80 s intervals, obtained in control and under 10 nM copper, for 46 well-sorted units, derived from eight experiments, ranked by its CSI. The average CSI was 0.62 ± 0.02 (dotted line: CSI = 0.5). (G) Distribution of CSI, continuous line represents best fit to Gaussian function (fitting parameters; centre = 0.615 ± 0.025; width = 0.195 ± 0.035). *indicates statistical significance evaluated to a significance level of $P \leq 0.05$.

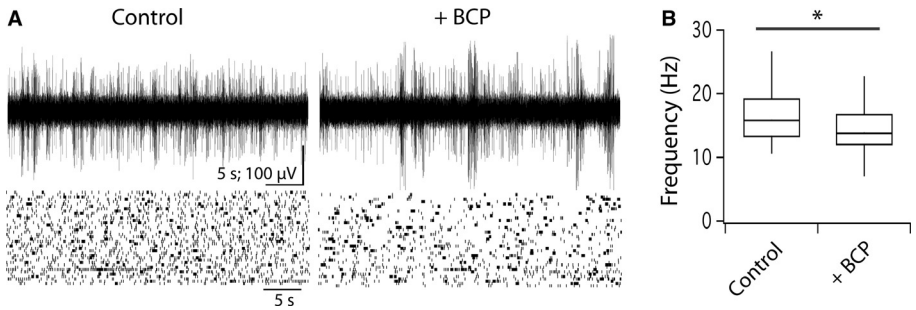

FIG. 10. Chelation of endogenous copper decreases spontaneous network activity. (A) Upper traces display extracellular recorded action potential (AP) trains with modified artificial cerebrospinal fluid (ACSF; control; left panel) and after bath-addition of bathocuproine (BCP; 20 μM, right panel). Lower panels show 40 raster plots summarizing spiking activity without and with copper chelating agent for a total of 160 s. (B) Box-plot summarizing the decrease of average AP frequency after BCP addition (in Hz: 16.82 ± 1.52 vs. 14.22 ± 1.43, $n = 12$, $P \leq 0.05$ *t*-test). *indicates statistical significance evaluated to a significance level of $P \leq 0.05$.

of unitary spikes in copper/total number of unitary spikes (control + copper). The index allows to establish whether a unitary spike decreased its frequency under copper ($0 < CSI < 0.5$), increased it ($0.5 < CSI < 1.0$), was not affected ($CSI = 0.5$) or was recruited in its presence ($CSI = 1$). To answer the question, the spiking activity was sorted in 80-s windows for each condition and the CSI calculated for each class of units. For the recordings shown in Fig. 9A, four different spike classes were found whose profile and frequency are shown in Fig. 9E. In Fig. 9F, the raster plots of 46 unitary spikes collected in eight different experiments for control and after copper addition were shown, sorted according to their CSI. There is no correlation between CSI and the average control spike rate ($r^2 = 0.047$), suggesting that Cu^{2+}-mediated enhancement is consistent with a linear scaling of synaptic drive reaching active neurons. In the presence of 10 nM Cu^{2+}, the CSI averaged 0.62 (Fig. 9G), an indication that most neurons enhanced their basal activity. Only three units out of 46 presented $CSI > 0.9$, therefore the fraction of units recruited by copper is 6.5%.

Copper chelation decreases spontaneous spiking activity in the active hippocampus network

A slight decrease in the divalent cations together with a 1 mM increase in K^+ concentration of ACSF induces slow rhythmic oscillations that mimic *in vivo* cortical and hippocampal activity (Sanchez-Vives & McCormick, 2000; Fanselow & Connors, 2010). The modified ACSF was used to address whether copper removal by BCP affects network activity. Modified ACSF produces a 5–10-fold increase in spontaneous spike frequency that is effectively decreased by 20 μM BCP (Fig. 10A and B; control: 16.8 ± 1.5 Hz; BCP: 14.2 ± 1.4 Hz, $n = 12$, $P \leq 0.05$ *t*-test), suggesting that endogenous copper regulates the spiking activity in the active hippocampus network. Therefore, it was considered that in natural conditions there is a background extracellular copper level that participates in regulating network activity. Furthermore, as copper removal decreases network activity, copper-induced enhancement described here has physiological relevance.

Discussion

An important contribution of this work is the operationally based estimation of extracellular copper levels in the CA1 area. A literature survey reports total copper concentrations of 10–25 μM for blood serum, 0.5–2.5 μM for cerebrospinal fluid and 30 μM for the synaptic cleft (Bush, 2000). The current data indicate that 10 nM copper produces a 40% activity enhancement of network activity (Fig. 9). This observation tells us that extracellular free copper concentration cannot be in the micromolar range, as 10 nM would be an insignificant concentration change. A rough functional estimate of background copper concentration can be made using the experimental data. Reduction to zero by copper chelating agent BCP produces a 15% decrease in network activity. Assuming that network activity is a linear function of copper concentration and the slope is 4% change in activity per nM copper, then 15% change in network activity corresponds to a 3.75 nM change in copper concentration. This calculation places the endogenous free copper concentration at about 4 nM at the extracellular fluid. Nanomolar copper concentrations at the extracellular space are reasonably possible as the copper concentration at the synaptic cleft could reach up to micromolar levels (Kozma *et al.*, 1981; Hartter & Barnea, 1988; Bush, 2000; Hopt *et al.*, 2003; Gaier *et al.*, 2013). Interestingly, activity enhancement by copper is 1% per nM when measured intracellularly as the shift in *f–I* curve or AP generation in near-threshold conditions (Figs 3C and 4E); a value that is only 25% of the one obtained at the network level. This indicates that copper effects at the network level include more than the simple change in excitability at the single cell level. Taken together, data from Figs 4, 9 and 10 indicate that the neuromodulatory effects of copper occur at nanomolar concentrations; higher concentrations may trigger harmful actions of copper.

Despite the well-known metabolic functions of copper (Lutsenko *et al.*, 2010; Gaier *et al.*, 2013) and its earlier association with neurological disorders (Wilson, 1912; Menkes *et al.*, 1962), its neurophysiological roles in normal and pathological conditions have remained elusive. Here it was shown that copper produces a variety of neural effects: enhances network activity, hyperpolarizes V_{th}, modulates AP CA1 conductances, makes the CA3–CA1 pathway gain highly variable, enhances neurotransmitter release, decreases inhibition and improves AP timing reliability, while leaving *f–I* gain and short-term plasticity untouched. Many of these effects could be explained by a documented interaction between copper and Hodgkin–Huxley conductances (Delgado *et al.*, 2006). In fact, a realistic simulation (Fig. 1) shows how small variations (5–10%) in the activation and inactivation kinetics of AIS sodium currents change V_{th}, a key parameter, that could explain the effects found at the cellular, synaptic and network levels. To better understand the neurophysiological functions of copper, the effects of copper are separated into two dimensions: activity enhancement and temporal processing effects. The simulations show that by modulating axonal channel kinetics, both V_{th} hyperpolarization (compare Fig. 1E with

Fig. 2C) and the invariance of the *f–I* transfer function gain can be mimicked (compare Fig. 1G with Fig. 3C). Activation and inactivation kinetics of axonal sodium currents account for 0.2 mV of V_{th} hyperpolarization per 1% change of sodium current kinetic acceleration. Thus, it seems plausible that the interaction between copper and the sodium channels located on the AIS is the basis of the effect of copper on intrinsic excitability regulation. This interaction could have important regulatory functions; therefore, further studies should specifically aim to unveil the details of such a relationship.

Next, the effects of copper are reviewed in more detail. A first interesting point is that V_{th} hyperpolarization by copper shows a linear dependency with copper concentration in the nM range, allowing an analogical tuning of neuronal excitability (Fig. 2D). A second copper effect is the shortening of the AP repolarization phase allowing higher discharge rates and permitting higher dynamic ranges (Fig. 2B and C). These two effects show that copper modulates intrinsic mechanisms responsible for AP generation and propagation that define the moment-by-moment local membrane dynamics. Thus, when V_m fluctuates near V_{th}, copper induces higher discharge rates by lowering V_{th} as well as by modifying the non-linear behaviour of V_m (Figs 2–4). Additionally, copper's spatial modulation of membrane conductances might allow differential control of neural excitability over distinct subcellular domains. Consequently, the AIS and other axonal domains are of special interest because in these regions the precise balance between ionic conductances defines moment-by-moment the segment excitability.

A third excitability effect was the upward shifting of the CA1 *f–I* input–output transfer function, while maintaining gain, a result theoretically predicted (Fig. 1G) and experimentally observed (Fig. 3C). The current results show that copper enhances neuronal output responses (by factors as large as 100–200%), while leaving encoding properties (represented by neuronal gain) intact. This copper-dependent enhancement not only overcomes frequency saturation constraints by allowing a larger output range, but also permits input trains having higher discharge rates to be processed with equal gain by CA1 neurons.

A fourth excitability effect was copper's activation of a higher number of presynaptic release sites almost doubling the frequency of asynchronous spontaneous EPSCs recorded at CA1 neurons (Fig. 5). Synaptic bombardment is significantly increased (by almost 70% by 50 nM copper), and it could be explained by the extra neural network activity induced by copper (Fig. 9). This is an important systemic effect, as synaptic integration of additional EPSCs will contribute to V_m depolarization making neurons more excitable especially if copper additionally hyperpolarized V_{th}. As copper is released by depolarization (Hartter & Barnea, 1988; Kardos *et al.*, 1989; Schlief & Gitlin, 2006; Schlief *et al.*, 2006; Tamano & Takeda, 2011), the enhancement of total EPSCs by copper opens a very interesting situation of self-reference stabilized positive feedback. In effect, after copper is released (somatic or synaptic release) it could reach the AIS via spillover or diffusion, and modulate V_{th} hyperpolarization similarly as a volume-transmitting agent (Agnati *et al.*, 2010; Trueta & De-Miguel, 2012). The extra activity thus generated will increase synaptic release across the network, and thus more copper will be available for spillover increasing even further neural activity. Therefore, normal copper homeostatic mechanisms should couple neuronal activity and extracellular copper levels within a tight functional range.

A fifth effect consists in altering the gain of the CA3 → CA1 pathway. While copper produces small enhancements in the recruitment of Schaffer collaterals (up to 50% in some cases), a substantial variability in the accompanying evoked synaptic field potential in the presence of 10, 50 or 100 nM copper (Fig. 6) was detected. After the addition of exogenous copper, the input/output gain changed in variable amounts indicating that copper targets a heterogeneous population of CA3 → CA1 synapses. The copper synaptic effects contribute to a network-wide increment in CA1 output by enhancing presynaptic bombardment and producing a heterogeneous recruitment of Schaffer collaterals. Interestingly, these synaptic effects do not interfere with calcium-dependent short-term synaptic plasticity (Fig. 7). The five enhancement effects thus far detailed, although operating at different levels (from axonal conductances to synaptic mechanisms), show that copper has a net effect of increasing the frequency range of CA1 neurons, while leaving the basic CA1 transfer function gain invariant.

Now the other area of copper's neurophysiological activity is considered: copper's effect on temporal processing (Buzsaki, 2010). Improvement in AP timing reliability near to V_{th} may constitute an important dimension of copper neuromodulatory role, because it minimizes timing errors for the generation of APs for a wide range of inputs and network activity levels (Fig. 4). Minimization of spike-timing errors improves the quality of the temporal structure of neural signals travelling through and generated in the hippocampus, as higher spike reliability, hence less timing-noise, translates into more coherent network activity.

Another timing effect involves a variety of inhibitory circuit configurations: feedback and feedforward inhibition and more complex arrangements that are so central at the hippocampal processing capabilities; this complexity has been embodied in the concept of an inhibitory matrix (Klausberger & Somogyi, 2008). The inhibitory matrix drives pyramidal cells and regulates fundamental aspects of neural processing, such as production of correlations and the generation of neural synchrony (Bartos *et al.*, 2007; Klausberger & Somogyi, 2008). The current results indicate that copper modulates this inhibitory matrix by depressing the inhibition reaching CA1 pyramidal neurons (Fig. 8A and B). Inhibition results from inhibitory interneurons that are activated through Schaffer collaterals (feedforward) or indirectly after CA1 pyramidal cells activation (feedback; Andersen *et al.*, 1963, 1964; Alger & Nicoll, 1982; Buzsaki, 1984; Deuchars & Thomson, 1996; Gulyas *et al.*, 1999; Pouille & Scanziani, 2001; Klausberger & Somogyi, 2008). After a Schaffer collateral stimulation, the time to first spike is determined by a perturbation of the excitation/inhibition balance. Therefore, the current data suggest that copper affects mainly feedforward inhibition (Fig. 8). The time to the first spike in the current experiments is proportional to stimulation intensity, i.e. proportional to the number of synaptic contacts activated in parallel. On the other hand, the feedback components are disynaptically driven requiring sequential CA1 activation; however, CA1 is silent during the time to first spike. Considering that the gain of the input/output does not change in the presence of copper, it is thought that copper attenuates the inhibitory drive. The IC_{50} for copper inhibition of $GABA_A$ receptors is 35 nM; in the current experiments the inhibitory component affected is the same for two copper concentrations around IC_{50}, suggesting that copper acts mainly at the circuit level and not by blocking $GABA_A$ receptors (Fig. 8).

The possibility of feedforward inhibition depression by copper is important as feedforward inhibition tends to decorrelate neural signals (Middleton *et al.*, 2012), thus to degrade temporal processing. Then, copper's moment-by-moment modulation of the inhibitory matrix in the extracellular three-dimensional spaces boosts correlation extraction by minimizing inhibition reaching pyramidal neurons. Additionally, copper also facilitates correlation extraction (along with improving reliability and diminishing inhibition) by

increasing cellular and synaptic components throughout the network. In effect, V_{th} hyperpolarization and increased excitatory synaptic bombardment decrease membrane potential difference between V_m and V_{th}, thus facilitating the temporal integration of presynaptic activity and thus, indirectly, the extraction of correlations across the network.

Considering the above results, it was proposed that in the hippocampal formation copper provides an activity tonus that controls excitability, and a correlation tonus that defines a system set-point for correlations to operate. It is believed that copper is at the core of a positive feedback loop that relates to a background level of physiological copper (Fig. 10). This background level of physiological copper must be submitted to tight control by the homeostatic mechanisms that maintain copper concentration in the nanomolar range. The neurological high-level functional effects of copper, by enhancing activity and boosting correlation extraction, reveal copper as a crucial functional component of the hippocampal circuitry.

Acknowledgements

The authors thank Ignacio Diaz and Jorge Vera for valuable help on some control experiments, Flavio Frohlich for helpful comments, Julio Alcayaga for suggestions about the statistical analysis, and Diane Greenstein for invaluable editorial assistance. Fondecyt 1080670, Enlace DI 2007 to C.V. This study was supported in part by a grant from FRAXA Research Foundation to C.M. None of the author declares a conflict of interest.

Abbreviations

ACSF, artificial cerebrospinal fluid; AIS, axonal initial segment; AP, action potential; BCP, bathocuproinedisulphonic acid; CSI, copper sensitivity index; EPSC, excitatory postsynaptic current; fEPSP, field excitatory postsynaptic potential; GABA, γ-aminobutyric acid; LFS, low-frequency stimulation; TTX, tetrodotoxin.

References

Aedo, F., Delgado, R., Wolff, D. & Vergara, C. (2007) Copper and zinc as modulators of neuronal excitability in a physiologically significant concentration range. *Neurochem. Int.*, **50**, 591–600.

Agnati, L.F., Guidolin, D., Guescini, M., Genedani, S. & Fuxe, K. (2010) Understanding wiring and volume transmission. *Brain Res. Rev.*, **64**, 137–159.

Alger, B. & Nicoll, R. (1982) Feed-forward dendritic inhibition in rat hippocampal pyramidal cells studied in vitro. *J. Physiol.*, **328**, 105–123.

Andersen, P., Eccles, J. & Loyning, Y. (1963) Recurrent inhibition in the hippocampus with identification of the inhibitory cell and its synapses. *Nature*, **198**, 540–542.

Andersen, P., Eccles, J. & Loyning, Y. (1964) Pathway of postsynaptic inhibition in the hippocampus. *J. Neurophysiol.*, **27**, 608–619.

Banci, L., Bertini, I., Cantini, F. & Ciofi-Baffoni, S. (2010) Cellular copper distribution: a mechanistic systems biology approach. *Cell. Mol. Life Sci.*, **67**, 2563–2589.

Bartos, M., Vida, I. & Jonas, P. (2007) Synaptic mechanisms of synchronized gamma oscillations in inhibitory interneuron networks. *Nat. Rev. Neurosci.*, **8**, 45–56.

de Bie, P., Muller, P., Wijmenga, C. & Klomp, L. (2007) Molecular pathogenesis of Wilson and Menkes disease: correlation of mutations with molecular defects and disease phenotypes. *J. Med. Genet.*, **44**, 673–688.

Bush, A.I. (2000) Metals and neuroscience. *Curr. Opin. Chem. Biol.*, **4**, 184–191.

Buzsaki, G. (1984) Feed-forward inhibition in the hippocampal formation. *Prog. Neurobiol.*, **22**, 131–153.

Buzsaki, G. (2010) Neural syntax: cell assemblies, synapsembles, and readers. *Neuron*, **68**, 362–385.

Chen, C. & Regehr, W. (1999) Contributions of residual calcium to fast synaptic transmission. *J. Neurosci.*, **19**, 6257–6266.

Davies, K.M., Hare, D.J., Cottam, V., Chen, N., Hilgers, L., Halliday, G., Mercer, J.F. & Double, K.L. (2013) Localization of copper and copper transporters in the human brain. *Metallomics*, **5**, 43–51.

Delgado, R., Vergara, C. & Wolff, D. (2006) Divalent cations as modulators of neuronal excitability: emphasis on copper and zinc. *Biol. Res.*, **39**, 173–182.

Deuchars, J. & Thomson, A. (1996) CA1 pyramid–pyramid connections in rat hippocampus in vitro: dual intracellular recordings with biocytin filling. *Neuroscience*, **74**, 1009–1018.

Dittman, J., Kreitzer, A. & Regehr, W. (2000) Interplay between facilitation, depression, and residual calcium at three presynaptic terminals. *J. Neurosci.*, **20**, 1374–1385.

Fanselow, E.E. & Connors, B.W. (2010) The roles of somatostatin-expressing (GIN) and fast-spiking inhibitory interneurons in UP-DOWN states of mouse neocortex. *J. Neurophysiol.*, **104**, 596–606.

Gaier, E.D., Eipper, B.A. & Mains, R.E. (2013) Copper signaling in the mammalian nervous system: synaptic effects. *J. Neurosci. Res.*, **91**, 2–19.

Gaier, E.D., Eipper, B.A. & Mains, R.E. (2014a) Pam heterozygous mice reveal essential role for Cu in amygdalar behavioral and synaptic function. *Ann. N.Y. Acad. Sci.*, **1314**, 15–23.

Gaier, E.D., Rodriguiz, R.M., Zhou, J., Ralle, M., Wetsel, W.C., Eipper, B.A. & Mains, R.E. (2014b) In vivo and in vitro analyses of amygdalar function reveal a role for copper. *J. Neurophysiol.*, **111**, 1927–1939.

Gruss, M., Mathie, A., Lieb, W.R. & Franks, N.P. (2004) The two-pore-domain K(+) channels TREK-1 and TASK-3 are differentially modulated by copper and zinc. *Mol. Pharmacol.*, **66**, 530–537.

Gulyas, A., Megias, M., Emri, Z. & Freund, T. (1999) Total number and ratio of excitatory and inhibitory synapses converging onto single interneurons of different types in the CA1 area of the rat hippocampus. *J. Neurosci.*, **19**, 10082–10097.

Hamill, O., Marty, A., Neher, E., Sakmann, B. & Sigworth, F. (1981) Improved patch-clamp techniques for high-resolution current recording from cells and cell-free membrane patches. *Pflug. Arch.*, **391**, 85–100.

Hartter, D.E. & Barnea, A. (1988) Evidence for release of copper in the brain: depolarization-induced release of newly taken-up 67copper. *Synapse*, **2**, 412–415.

Herms, J., Tings, T., Gall, S., Madlung, A., Giese, A., Siebert, H., Schurmann, P., Windl, O., Brose, N. & Kretzschmar, H. (1999) Evidence of presynaptic location and function of the prion protein. *J. Neurosci.*, **19**, 8866–8875.

Hopt, A., Korte, S., Fink, H., Panne, U., Niessner, R., Jahn, R., Kretzschmar, H. & Herms, J. (2003) Methods for studying synaptosomal copper release. *J. Neurosci. Meth.*, **128**, 159–172.

Hu, W., Tian, C., Li, T., Yang, M., Hou, H. & Shu, Y. (2009) Distinct contributions of Na(v)1.6 and Na(v)1.2 in action potential initiation and backpropagation. *Nat. Neurosci.*, **12**, 996–1002.

Huidobro-Toro, J., Lorca, R. & Coddou, C. (2008) Trace metals in the brain: allosteric modulators of ligand-gated receptor channels, the case of ATP-gated P2X receptors. *Eur. Biophys. J.*, **37**, 301–314.

Kardos, J., Kovacs, I., Hajos, F., Kalman, M. & Simonyi, M. (1989) Nerve endings from rat brain tissue release copper upon depolarization. A possible role in regulating neuronal excitability. *Neurosci. Lett.*, **103**, 139–144.

Klausberger, T. & Somogyi, P. (2008) Neuronal diversity and temporal dynamics: the unity of hippocampal circuit operations. *Science*, **321**, 53–57.

Kole, M., Ilschner, S., Kampa, B., Williams, S., Ruben, P. & Stuart, G. (2008) Action potential generation requires a high sodium channel density in the axon initial segment. *Nat. Neurosci.*, **11**, 178–186.

Kozma, M., Szerdahelyi, P. & Kasa, P. (1981) Histochemical detection of zinc and copper in various neurons of the central nervous system. *Acta Histochem.*, **69**, 12–17.

Lalioti, V., Muruais, G., Tsuchiya, Y., Pulido, D. & Sandoval, I.V. (2009) Molecular mechanisms of copper homeostasis. *Front Biosci.*, **14**, 4878–4903.

Letelier, J.C. & Weber, P.P. (2000) Spike sorting based on discrete wavelet transform coefficients. *J. Neurosci. Meth.*, **101**, 93–106.

Lorca, R.A., Coddou, C., Gazitua, M.C., Bull, P., Arredondo, C. & Huidobro-Toro, J.P. (2005) Extracellular histidine residues identify common structural determinants in the copper/zinc P2X2 receptor modulation. *J. Neurochem.*, **95**, 499–512.

Lutsenko, S. (2010) Human copper homeostasis: a network of interconnected pathways. *Curr. Opin. Chem. Biol.*, **14**, 211–217.

Lutsenko, S., Bhattacharjee, A. & Hubbard, A.L. (2010) Copper handling machinery of the brain. *Metallomics*, **2**, 596–608.

Menkes, J.H., Alter, M., Steigleder, G.K., Weakley, D.R. & Sung, J.H. (1962) A sex-linked recessive disorder with retardation of growth, peculiar hair, and focal cerebral and cerebellar degeneration. *Pediatrics*, **29**, 764–779.

Middleton, J.W., Omar, C., Doiron, B. & Simons, D.J. (2012) Neural correlation is stimulus modulated by feedforward inhibitory circuitry. *J. Neurosci.*, **32**, 506–518.

Niciu, M.J., Ma, X.M., El Meskini, R., Ronnett, G.V., Mains, R.E. & Eipper, B.A. (2006) Developmental changes in the expression of ATP7A during a critical period in postnatal neurodevelopment. *Neuroscience*, **139**, 947–964.

Pase, L., Voskoboinik, I., Greenough, M. & Camakaris, J. (2004) Copper stimulates trafficking of a distinct pool of the Menkes copper ATPase (ATP7A) to the plasma membrane and diverts it into a rapid recycling pool. *Biochem. J.*, **378**, 1031–1037.

Pouille, F. & Scanziani, M. (2001) Enforcement of temporal fidelity in pyramidal cells by somatic feed-forward inhibition. *Science*, **293**, 1159–1163.

Prohaska, J.R. (1987) Functions of trace elements in brain metabolism. *Physiol. Rev.*, **67**, 858–901.

Que, E.L., Domaille, D.W. & Chang, C.J. (2008) Metals in neurobiology: probing their chemistry and biology with molecular imaging. *Chem. Rev.*, **108**, 1517–1549.

Saito, T., Itoh, T., Fujimura, M. & Saito, K. (1995) Age-dependent and region-specific differences in the distribution of trace elements in 7 brain regions of Long-Evans Cinnamon (LEC) rats with hereditary abnormal copper metabolism. *Brain Res.*, **695**, 240–244.

Sanchez-Vives, M. & McCormick, D. (2000) Cellular and network mechanisms of rhythmic recurrent activity in neocortex. *Nat. Neurosci.*, **3**, 1027–1034.

Schlief, M. & Gitlin, J. (2006) Copper homeostasis in the CNS: a novel link between the NMDA receptor and copper homeostasis in the hippocampus. *Mol. Neurobiol.*, **33**, 81–90.

Schlief, M.L., Craig, A.M. & Gitlin, J.D. (2005) NMDA receptor activation mediates copper homeostasis in hippocampal neurons. *J. Neurosci.*, **25**, 239–246.

Schlief, M.L., West, T., Craig, A.M., Holtzman, D.M. & Gitlin, J.D. (2006) Role of the Menkes copper-transporting ATPase in NMDA receptor-mediated neuronal toxicity. *Proc. Natl. Acad. Sci. USA*, **103**, 14919–14924.

Schreiber, S., Fellous, J.M., Whitmer, D., Tiesinga, P. & Sejnowski, T.J. (2003) A new correlation-based measure of spike timing reliability. *Neurocomputing*, **52–54**, 925–931.

Sharonova, I.N., Vorobjev, V.S. & Haas, H.L. (1998) High-affinity copper block of GABA(A) receptor-mediated currents in acutely isolated cerebellar Purkinje cells of the rat. *Eur. J. Neurosci.*, **10**, 522–528.

Sharonova, I.N., Vorobjev, V.S. & Haas, H.L. (2000) Interaction between copper and zinc at GABA(A) receptors in acutely isolated cerebellar Purkinje cells of the rat. *Brit. J. Pharmacol.*, **130**, 851–856.

Tamano, H. & Takeda, A. (2011) Dynamic action of neurometals at the synapse. *Metallomics*, **3**, 656–661.

Tarohda, T., Yamamoto, M. & Amamo, R. (2004) Regional distribution of manganese, iron, copper, and zinc in the rat brain during development. *Anal. Bioanal. Chem.*, **380**, 240–246.

Trueta, C. & De-Miguel, F.F. (2012) Extrasynaptic exocytosis and its mechanisms: a source of molecules mediating volume transmission in the nervous system. *Front. Physiol.*, **3**, 319.

Vogt, S. & Ralle, M. (2013) Opportunities in multidimensional trace metal imaging: taking copper-associated disease research to the next level. *Anal. Bioanal. Chem.*, **405**, 1809–1820.

Wilson, S.A.K. (1912) Progressive lenticular degeneration: a familiar nervous disease associated with cirrhosis of liver. *Brain*, **34**, 295–507.

Xiao, Z., Brose, J., Schimo, S., Ackland, S.M., La Fontaine, S. & Wedd, A.G. (2011) Unification of the copper(I) binding affinities of the metallochaperones Atx1, Atox1, and related proteins. *J. Biol. Chem.*, **286**, 11047–11055.

Yamada, Y. & Prosser, R.A. (2014) Copper chelation and exogenous copper affect circadian clock phase resetting in the suprachiasmatic nucleus in vitro. *Neuroscience*, **256**, 252–261.

Zatta, P. & Frank, A. (2007) Copper deficiency and neurological disorders in man and animals. *Brain Res. Rev.*, **54**, 19–33.

Zucker, R. & Regehr, W. (2002) Short-term synaptic plasticity. *Annu. Rev. Physiol.*, **64**, 355–405.